Hindawi Publishing Corporation
Advances in Mechanical Engineering
Volume 2012, Article ID 519471, 18 pages
doi:10.1155/2012/519471

Research Article

Modeling and Calibration for Crack Detection in Circular Shafts Supported on Bearings Using Lateral and Torsional Vibration Measurements

A. Tlaisi, A. S. J. Swamidas, M. R. Haddara, and A. Akinturk

Faculty of Engineering and Applied Science, Memorial University of Newfoundland, St. John's, NL, Canada A1B 3X5

Correspondence should be addressed to A. Tlaisi, atlaisi@mun.ca

Received 10 June 2011; Revised 25 September 2011; Accepted 14 October 2011

Academic Editor: A. Seshadri Sekhar

In this paper the requisite foundational numerical and experimental investigations that are carried out, to model the "uncracked and cracked" shaft and to identify its bending and torsional vibration responses, are reported. The cylindrical shaft used in this experimental study is continuous over two spans (with a cantilever span carrying a propeller) with ball-bearing supports. During modal tests the backward end of shaft (away from the propeller end and connecting it to an electric motor, required for online monitoring) is fixed to one of the test frame supports; later on this backward end will be connected to an electric motor to carry out online modal monitoring for crack identification. In the numerical study, beam elements are used for modeling the bending and torsional vibrations of the rotating shaft. The paper describes in detail the numerical "linear spring" models developed for representing the effects of "ball bearings and the (experimental test) frame supports" on the vibration frequencies. Shaft response parameters are obtained using modal analysis software, LMS Test Lab, for bending vibrations monitored using accelerometers, and three "sets" of shear strain gages fixed at three different shaft locations measure the torsional vibrations. Effects of different crack depths on bending and torsional frequencies and mode shapes are investigated experimentally and numerically, and the results interpreted to give better comprehension of its vibratory behavior.

1. Introduction

Vibration and noise in industrial machines, or in the environment around them, occur when dynamic forces excite these machines. This industrial noise has direct and indirect effects on the health and safety of those operating them. They can also have effects on buildings, machinery, equipment, and vehicles around them. These effects usually manifest themselves in the form of reduced performance, wear and tear, faulty operation, and irreversible damage in the form of cracks.

In the last four decades [1, 2], the vibrational behavior of cracked shafts has received considerable attention in order to prevent significant rotor faults, which can lead to catastrophic failures if undetected. The diagnosis of these cracked shafts remains problematic. In general cases, the behavior of the shaft is insensitive to a crack. Sometimes, it is difficult to find differences between successive states of vibration, even if the crack is medium sized. Thus, it is of the utmost importance to discover the identifiable specific characteristics of the cracked shaft at the earlier possible instance.

There are two stages in crack development: crack initiation and crack propagation. The former is caused by mechanical stress raisers, such as sharp keyways, abrupt cross-sectional changes, heavy shrink fits, dents and grooves, and/or metallurgical factors, such as flows, fretting, and forging. The latter stage, namely, crack propagation, can accelerate the growth rate under different conditions: operating faults generated during sustained surging in compressors' negative sequence current or grounding faults in generators and coupled turbines, the presence of residual stresses in the rotor material, thermal stresses, and environmental conditions, such as the presence of a corrosive medium. Cracks can be classified based on their geometry and orientation as follows: cracks perpendicular to the shaft axis are known as transverse cracks; cracks parallel to the shaft axis are known as longitudinal cracks; cracks at an angle to the shaft axis are known as slant cracks; cracks that open and close, when the

affected part of the material is subjected to alternating stresses, are known as breathing cracks; cracks that primarily remain open are known as gaping cracks or notches; cracks that appear open on the surface are known as surface cracks; cracks which are not visible on the surface are known as subsurface cracks [3].

1.1. Literature Review. Munoz et al. [4] applied a modal testing procedure to detect a crack on an offline rotor. The changes in rotating shaft frequencies gave a good indication of the presence of cracks. They stated that the method can be used to detect cracks of areas greater than 2.5% of the rotor cross-sectional area, but this claim seems to be rather exaggerated from other studies published on the same.

Gounaris and Papadopoulos [5] performed experiments using a rotating cracked shaft. The shaft was excited at one end, and the response was measured at the other end. Hamidi et al. [6] developed two mathematical models to determine the bending natural frequencies of a rotor. The analytical results were compared with the results of experiments. The following conclusions were made. (i) When crack depth was more than 30% of the shaft radius, the rate of change of the natural frequency was high. (ii) The speed of the rotating shaft did not affect the values of the natural frequency: this was probably due to the fact that stiffness of the rotating shaft system is governed by the shaft stiffness which is not influenced by the rotational speed of the shaft. Tsai and Wang [7] used transfer matrix method on the basis of Timoshenko beam theory to obtain the dynamic characteristics and thereby identify the location and size of cracks based on monitoring the change in the mode shapes and natural frequencies of a cracked shaft. Their method was validated by comparison with existing published experimental data. Zakhezin and Malysheva [8] used a numerical finite element- (FE-) based crack detection technique and modal tests on a single span shaft. They included system damping in their model and calculated the system's natural frequencies, eigenvalues, and eigenvectors up to a frequency of 1100 Hz. These values were calculated for a rotor with and without cracks at varying locations and depths. The method was tested and results verified to demonstrate the good quality of results obtained.

Adewusi and Al-bedoor [9] applied neural networks techniques to detect the inception of cracks on rotors. They carried out experimental studies on a rotor (overhung arrangement and simply supported arrangement) with and without a propagating crack. In this study, a two neuron network was used to detect the propagating crack and a three neuron network to detect the propagating and nonpropagating cracks. Prabhakar et al. [10] investigated experimentally the influence of a transverse surface crack on the mechanical impedance of a rotor bearing system. This system consisted of rigid disks, distributed parameter finite shaft elements, and discrete bearings. The experimental work was done to validate their previous numerical analysis results. They tried to use the concept of mobility for detecting and monitoring the crack using different crack parameters and force locations. The authors did this experiment for an uncracked and a cracked shaft. They used different depths (20% and 40% of diameter to represent the crack depth) at the location. Also, they measured the mobility in two directions, horizontal and vertical, at the bearing locations. This measurement was taken at different rotor speeds. They found that the mobility was directly proportional to the depth of the crack, as well as to the rate of change of mobility at the running frequency. Moreover, since the crack depth was assumed to grow vertically, the rate of change of mobility in the vertical direction was greater than that in the horizontal direction. There was considerable agreement between experimental results and numerical simulations. Therefore, the authors suggest using this method to detect the crack and monitoring in a rotor-bearing system.

Pennacchi and Vania [11] presented the results of an experimental study concerning the diagnoses of a crack during the load coupling of a gas turbine; they compared the experimental and analytical results of the shaft vibration using the model of the rotating shaft of a 100 MW power plant. Dorfman and Trubelja [12] used a simplified model of the turbine generator system to examine the influence of cracks in the shaft. This model showed the relationship between the shaft excitation forces which represented input to the model and the shaft torsional vibration response which represented the output. This ratio (output to the input) is known as the transfer function. The transfer function is basically dependent on the mass, stiffness, and damping of the shaft. They found that a properly designed data acquisition monitoring system, such as structural integrity associate's transient torsional vibration monitor system (SI-TTVMS), would give a good signal and detect rotor faults before failure. Cho et al. [13] measured the torsional wave in the rotating shafts by using a noncontact method (magnetostrictive patches and a solenoid). In this work, two problems were noticed during vibration experiment, namely, (i) how to produce sufficient power to generate torsional waves; (ii) how to guarantee that there is no interference from the shaft rotational motion. Magnetostrictive patches were fastened indirectly to the shaft axis for measuring the torsional motion. Furthermore, the configuration of an arrayed patch was employed for frequency localization and sufficient power generation. In this paper, they assumed that the effect of the lateral vibrations was negligible because it was very small compared to the torsional motion measured by magnetostrictive strips. Also the authors used the transduction method to detect a perimeter crack in a rotating shaft as well as to estimate the damage location (with small error) and compare them with the exact crack size and location.

1.2. Scope of the Study. In the present paper, experimental and numerical investigations are carried out to identify the transverse crack existence in a cylindrical shaft with a cantilever overhang, using lateral and torsional vibrations. LMS experimental setup, described below, has been used for measuring the cracked and uncracked shaft response parameters. Effects of different crack depths are investigated experimentally and numerically. The shaft is fixed at one end to the test frame support and is continuous over the other frame support to end in a cantilevered end supporting the propeller; the shaft is supported through ball bearings that are attached to the two test frame supports, as shown in Figures 1

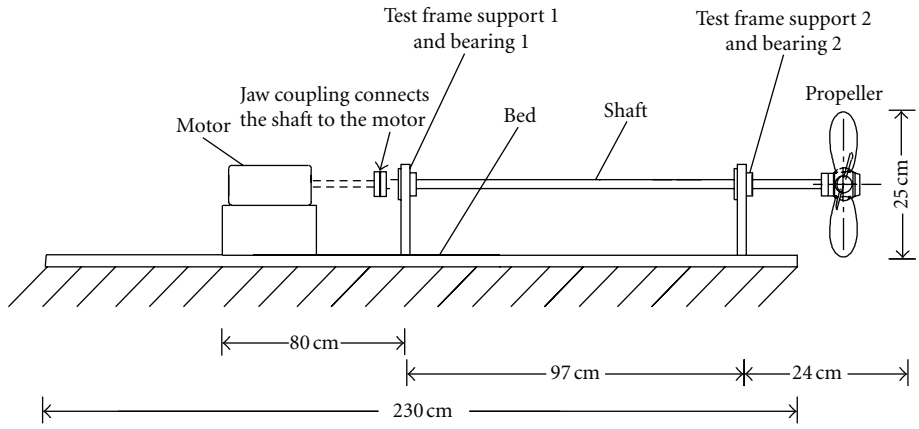

Figure 1: Schematic of uncracked shaft during online monitoring studies (the jaw coupling at the backside of bearing 1 is disconnected during modal tests).

and 2. Initially the cylindrical shaft, supported through roller bearings and test frame supports, had to be properly modeled for carrying out analysis using finite element procedures. The beam element, BEAM4, available in ANSYS finite element program is used for the numerical prediction of the dynamic response of uncracked and cracked shafts as well as to verify the experimental results. In this study, a linear "three-to-six-spring" model is used to represent the effects of each of the two ball bearings, supporting the shaft, over the (fixed) end and the other support with cantilever end; these spring constants are determined to achieve the best agreement between uncracked experimental and numerical results. Since the BEAM4 elements do not include the stress intensity effects present in cracks, an equivalent crack effect, as described by Petroski [14] and Rytter [15] with the use of a short beam element, is used in the present study to include the stress intensity effects in cracks. In addition since the propeller end will generate torsional motions of the shaft, detailed investigations were carried out to monitor the lower torsional frequency of the shaft and the crack influence at that frequency.

2. Theory and Modeling of the Bearing Support

One transverse open crack has been considered to be present in the shaft in this study. The uncracked shaft, shown in Figure 1, is modeled by replacing the bearing support effects by linear translational and rotational springs shown in Figure 2; the actual bearing support used in the experimental study is shown in Figure 3 (see McMaster-Carr, 2011 [16]). In the ball bearing used during these experiments, the flange of the housing bearing is fixed to the steel support frame; the inner ball bearing is fixed to the cylindrical shaft by tightening two screws positioned at 90° to one another. The elasticity of these bearing connections of the test frame supports and the cylindrical shaft are replaced by orthogonal linear springs, located at the positions of the two orthogonal tight screws. Hence the linear spring supports at right angles, used in this study, represent the effects of these tight screws of the cylindrical shaft (along with the flange mount and inner bearing), on the vibration frequencies of the shaft. Figures $2(a_1)$ to $2(e_1)$ show the five models used for modeling the ball bearing and test frame supports used in the study, namely, six, eight, ten, and twelve springs, respectively.

From the results obtained (shown later in the paper) it was observed that none of these five numerical models are fully sufficient to represent exactly the bearing support effects, but they do reasonably represent the effects of the bearing supports; as such they give reasonably good results when compared with the measured experimental results. For each spring support location the restoring forces increase or decrease depending on the deformation at that location, which in turn depend on the shaft and bearing influences at the same location. The best model that gives results very close to the experiment is identified in the subsequent computations given in a later section.

3. Modal Testing and Analysis of Cracked Shaft

In this part, the characteristics of the vibrating uncracked and cracked shaft are investigated through modal testing. Manually made saw cuts (0.65 mm wide) are used as cracks of different depths. The objective of this experimental study is to study the effect of cracks on the lateral and torsional vibrations of the tested cylindrical shaft. The experimental results are used to validate the most appropriate numerical model. The equipment system used to measure the two types of vibrations, namely, lateral and torsional modes of a cylindrical shaft system, is shown in Figure 4. For the experimental portion of the study, the engineering innovation (LMS Test Lab) software package with two measurement channels is used. The first input channel records the time history output from the modal hammer used in the study, shown in Figure 4(a). The number designation of the impact hammer type is 8206-002, and the maximum force (nondestructive) that it can deliver is 4448N.

The head of the hammer can use different tip materials, namely, aluminum, plastic, rubber, and stainless steel. In this study, plastic tip (DB-3991-002) material was used. The second channel records the time history output from the

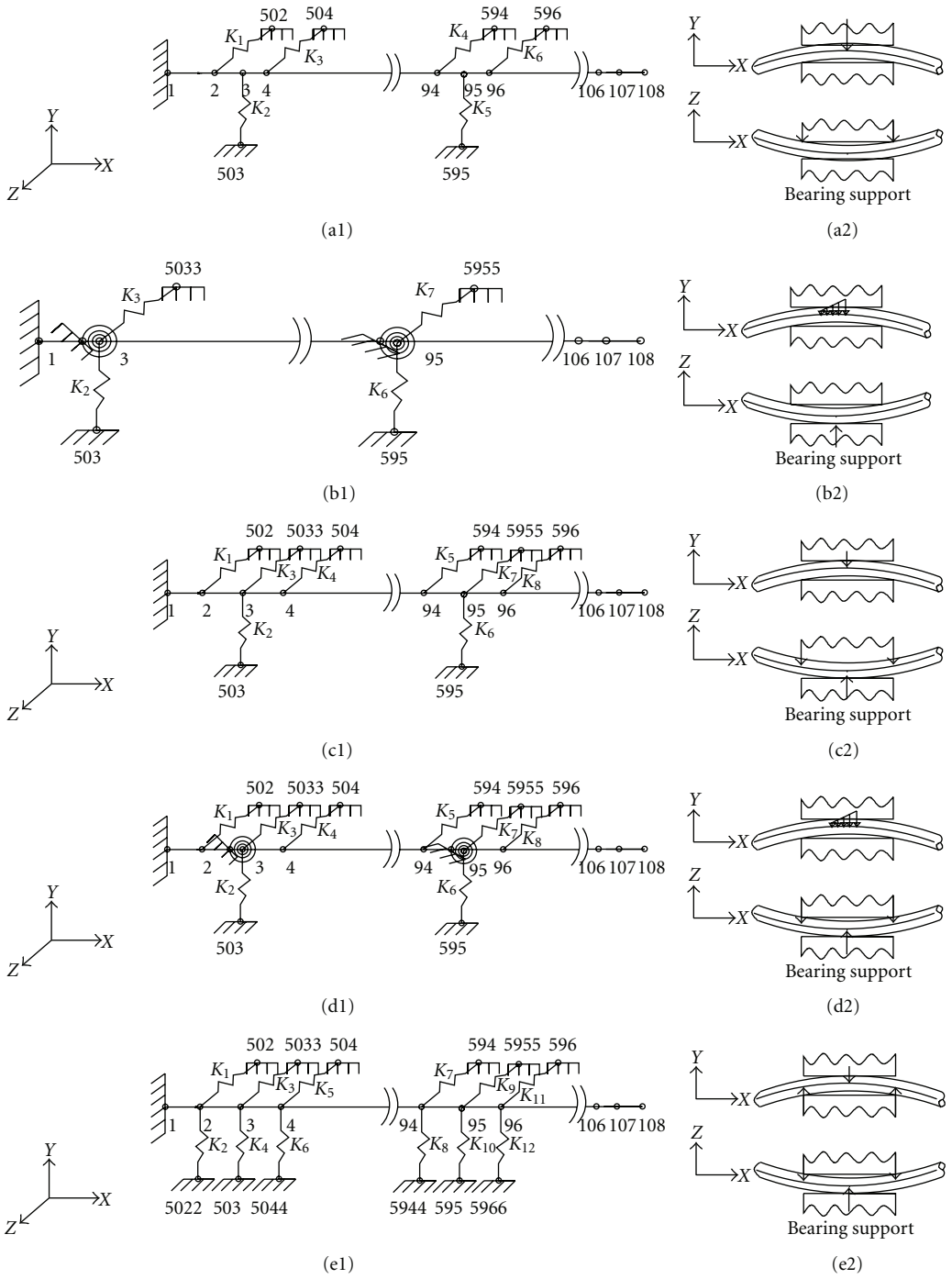

Figure 2: Finite element model for cylindrical shaft and bearings: (a_1) and (a_2) six translational springs modeling; (b_1) and (b_2) four translational and two rotational springs modeling; (c_1) and (c_2) eight translational springs modeling; (d_1) and (d_2) eight translational and two rotational springs modeling; (e_1) and (e_2) twelve translational springs modeling.

accelerometer device shown in Figure 4(b); alternately a set of shear strain gages can also be used instead of an accelerometer.

As shown in Figure 5(a), in subsequent online monitoring studies, the backside end of the continuous shaft with the cantilever overhang (in the forward end) will be connected to an electric motor and driven at a maximum speed of 4000 rpm, but, in the present experimental modal testing, the backside connection to the electric motor is disconnected and modal testing done in a "static" configuration of the cylindrical shaft. The propeller is attached to the overhanging end. During modal tests the shaft, with the overhang, is locked (or fixed) to the bearing support (bearing support 1) as shown in Figure 5(b). The fixed rotor shaft of 16 mm

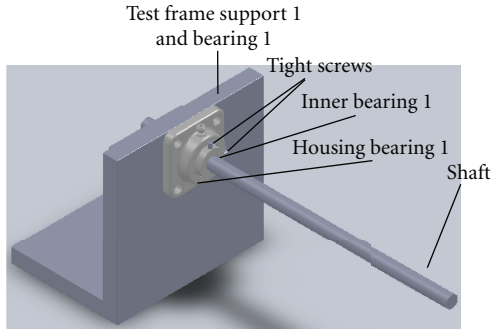

Figure 3: Schematic diagram of cylindrical shaft with mounted ball bearing.

diameter and 1210 mm length is supported on two bearings with greased fittings and deep-grooved ball-bearing inserts. Two set screws, separated by 90°, are used to fix the bearings to shaft at each of the bearings 1 and 2. The experimental program is carried out to identify the dynamic shaft characteristics with and without the presence of crack; a crack having different depths was made at 2.0 cm to the right of bearing number 2, as shown in Figure 5(c).

Figure 6 shows the experimental setup used to measure torsional vibration of the cylindrical shaft. In the torsional vibration measurement system three strain gages are fixed at three locations, one placed near the bearing support 1, the second placed at the middle of the supported span, and the last one placed near the propeller (in the overhanging end) as shown in Figure 6(a). Two sets of Suzette type (K-XY3X) model strain gauges with connection cables (4-wire circuit), fixed at three locations, are used. They are assembled in half bridge configurations. These sets of strain gauges are mounted 180° apart on the circumference of the shaft (along the neutral axis of the uncracked beam) at a given longitudinal location. The way they are oriented enables the measurement of torsional strains while any incidental strains due to beam bending cancel each other. Figures 6(c) and 6(d) show the sets of strain gauges used during modal tests and locations along the shaft. In Figure 6(d), c and d represent the size of strain gauge with high-endurance backing material (HBM); a, b_1, and b_2 the actual length and width of strain gauge wires. An aluminum arm is used to apply various magnitudes of impact torque at various locations of shaft. Five (multiplexed) data acquisition channels are used, namely, three for torque gages, one accelerometer (±4g's) channel, and the fifth for impact load with the modal hammer.

Neither ANSYS software package [17] nor the LMS Test Lab system was able to indicate the presence of the first torsional frequency in the shaft-propeller system. The probable reasons are as follows: (i) BEAM4 type beam element probably does not give the first torsional mode due to the improper lumped mass values used for torsional motions [17]; probably higher-order beam elements (such as BEAM-188 or BEAM189, having warping as an additional degree of freedom) would have given the first torsional frequency (this was not attempted since the use of warping as another variable, along with the available six degrees of freedom at a point, looked superfluous for the shaft vibration); (ii) the LMS Test Lab does not give the torsional mode since the accelerometer used (for getting the modal amplitudes) measured only the bending motions, and as well the LMS software used in the study does not attempt to extract from the torsional vibration features from the monitored vibration signals. Hence a different procedure had to be devised to determine the torsional frequency(s) of the shaft-propeller system. For the analytical portion of the investigation to calculate the natural frequency of torsional vibration, the rotational spring constant of the shaft and mass moment of inertia of a propeller (in addition to the aluminum plate used for generating sudden impact torsional moments in the shaft) about the axis of rotation had to be determined. Figure 7 shows a standard trifilar suspension arrangement that was used to determine the platform and propeller properties. This trifilar suspension structure is a circular, stiff, plywood platform attached and hooked to a hanger via stiffer ropes. The three ropes were fixed tight on the top to keep platform suspension as flat as possible. Also in this experiment, a stop watch was used to record the time of torsional oscillations.

The device shown in Figure 7 was used to determine the frequency of oscillation of the objects placed on the platform. By using two equations given below to calculate mass moment of inertia and by subtracting the mass moment of inertia of the platform from the mass moment of inertia of the combined object (propeller) and platform, the mass moment of inertia of the propeller can be determined [18]

$$J_{\text{cm}} = \frac{mgr^2}{L\omega_{\text{nd}^2}},$$
$$J_{\text{disk}} = (0.5)mr^2, \tag{1}$$

where J_{cm} is the mass moment of inertia for platform and object, J_{disk} is the theoretical value of mass moment of inertia of the platform disk, ω_{nd} is the torsional frequency of motion of the above device, for platform, and L is the length of the rope.

Now, the torsional natural frequency ω_n of the cylindrical shaft (with the propeller and the torsion impact device) is calculated by using this formula:

$$\omega_n = \left(\frac{Ks}{J_{\text{T}}}\right)0.5, \tag{2}$$

$$K_s = \frac{I_{\text{p}}G}{L_{\text{s}}}, \tag{3}$$

$$I_p = \frac{\pi d^4}{32}, \tag{4}$$

$$G = \frac{E}{2(1+\upsilon)}, \tag{5}$$

$$J_{\text{shaft}} = (0.5)Mr^2, \tag{6}$$

$$J_T = J_{\text{shaft}} + J_{\text{propeller}} + J_{\text{plate}}, \tag{7}$$

where K_s is the torsion stiffness of the shaft, J_T is total polar mass moment of inertia for shaft, propeller, and plate, I_p is the polar area moment of inertia of the shaft, L_s is the length

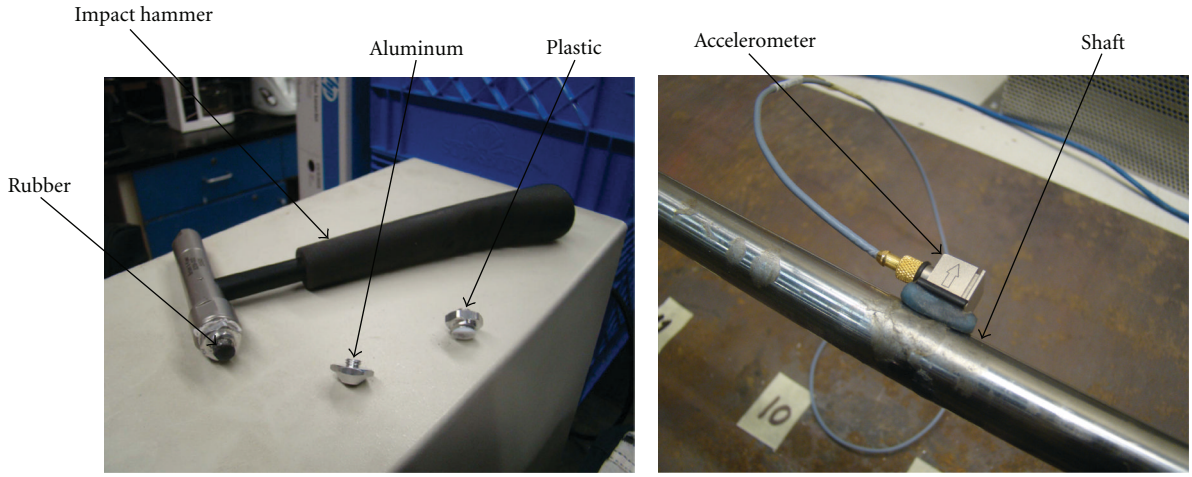

Figure 4: Photo of: (a) impact hammer and tips and (b) attached accelerometer.

of shaft, G is the shear modulus of the shaft, E modules of elasticity, v is the Poisson ratio of shaft material, J_{shaft} is polar mass moment of inertia for shaft, M is mass of shaft, r is the shaft radius, $J_{\text{propeller}}$ polar mass moment of inertia for propeller, and J_{plate} polar mass moment of inertia for the plate used for torsional impact.

4. Preparation for Modal Tests on Uncracked and Cracked Shafts

In the present investigation, the general aim is to identify the dynamic system characteristics when the damage (or crack) occurs on the cylindrical shaft. As mentioned above, the experimental investigation is carried out for crack detection, using only one crack location. In the numerical study, a number of cases are considered; one corresponding to the uncracked shaft and the other the cracked shaft having different crack depths. The crack is located at the maximum bending moment position, namely, on the right hand side of bearing support 2. Commercial ANSYS software is used to determine the dynamic characteristics so as to correlate them with the experimental results. In the finite element model the shaft was continuous over one support, namely, support 2 (having the overhanging span for propeller) with a ball bearing. The cylindrical shaft sketch is shown in Figure 8(a). Its right-hand side end (carrying the propeller) is free, while the left one (at support 1) is clamped. The length and the diameter of the shaft are as given above, that is, 1210 mm and 16 mm, respectively. The moment of inertia of the uncracked cross-section is $I = 3.217 \times 10^{-9}\,\text{m}^4$ and the polar moment of inertia for each element is $I_p = 6.434 \times 10^{-9}\,\text{m}^4$. The Young's modulus is $E = 2 \times 10^{11}\,\text{N/m}^2$, Poisson's ratio is 0.3, shear modulus of elasticity is $G = 7.69 \times 10^{10}\,\text{N/m}^2$, and the density is $p = 7667\,\text{kg/m}^3$. Beam element (BEAM4) was used to model the shaft used for numerical analysis through ANSYS. This element is a uniaxial element with torsion, bending, tension, and compression capabilities. The element has six degrees of freedom at each node: axial, transverse, and rotational motions are shown with numbering of its local degrees of freedom in Figure 7(b).

When modeling the shaft it is assumed that all the elements have the same material properties and geometrical profiles except at the cracked location, which has a different geometrical property (reduced stiffness) due to the presence of crack at that location. In this modeling, it is assumed that neutral axis does not shift at the crack location, which is not proper.

5. Presentation of the Results and Discussion

In this part of the study the findings from results obtained experimentally and numerically are presented and discussed. For experimental and numerical studies, one crack position and various crack ratios (from 0% to 70% ratio) are examined. From a detailed comparison of numerical results, obtained for six, eight, ten, and twelve springs modeling, with the experimental results for the uncracked rotor shaft, it is found that the six springs (shown in Figure 2(b), with some area of contact near the screwed inner bearing contact with the cylindrical shaft) model gave the smallest difference between the numerical and experimental frequency results. Hence the model with six springs (Figure 2(b)) is used as the proper model for subsequent studies; it is also observed from the ANSYS numerical results (using BEAM4 shaft elements) that the output did not contain any first torsional frequency; it did contain a higher torsional frequency at 652.0 Hz (which could not be the correct frequency value, since the BEAM4 formulation used in ANSYS does not properly compute contribution to the torsional moment of inertias). Table 1 shows the comparison of the first eight natural frequencies (four vertical and four horizontal) between the experimental and numerical values (uncracked and cracked), for the case of six springs (see Figure 2(b)). In this part of the study only one element, having a width of 0.65 mm (equal to the width of the saw-cut crack), is used to represent the crack, and all the other elements, around the crack region, are also similar to

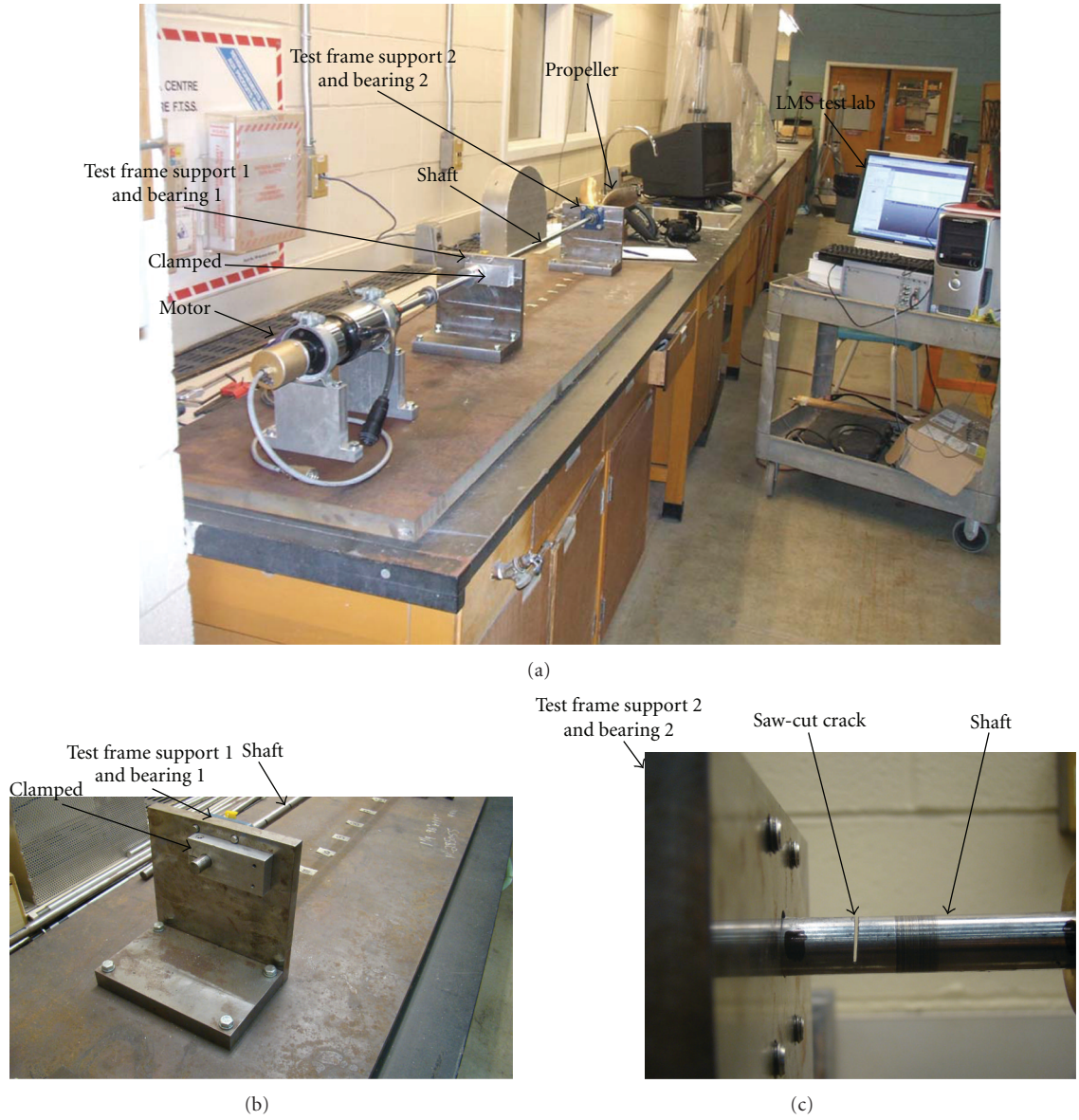

Figure 5: (a) LMS Test Lab with the shaft during modal tests; (b) the clamped end of the cylindrical shaft at bearing 1; (c) the saw-cut crack with 70% crack depth ratio.

(but wider than) this element. It can be seen from Table 1 that the experimental values show comparatively larger changes for the crack present in the shaft whereas the numerical analysis results show almost no changes, as the crack depth increases from 0 to 70%. The numerical analysis seems to be insensitive to the presence of the crack. This is due to the fact that the flexibility introduced in the experimental model by the presence of a crack seems to be much higher than that provided by the length size of 0.65 mm for a single finite element used to represent the crack effect in the numerical model, as shown in Figure 9(a). To improve the numerical results, the model shown in Figure 9(b) is used (where many elements of 0.65 mm length are used) to represent the crack effect. It is observed that even though a large number of smaller elements have been used to represent a single wider crack it has been found to give the same accuracy as the finite element model with a number of variable length elements. Table 1 shows the comparison of the first eight natural frequencies between the experimental and numerical results (with six springs) with the simulated correction with a larger number of small beam elements to represent crack. It shows from this comparison that the results of corrected numerical analysis are much closer to the experimental results.

Taking into consideration the representation of the crack by a modeled short beam element (having the same depth as the uncracked portion of shaft, at the cracked section, but with a larger element width—see Figure 9(b)) in the studies of Petroski [14] and Rytter [15] and the crack influence zone cited by Yang [19], more studies were carried out by considering additional elements around the crack location

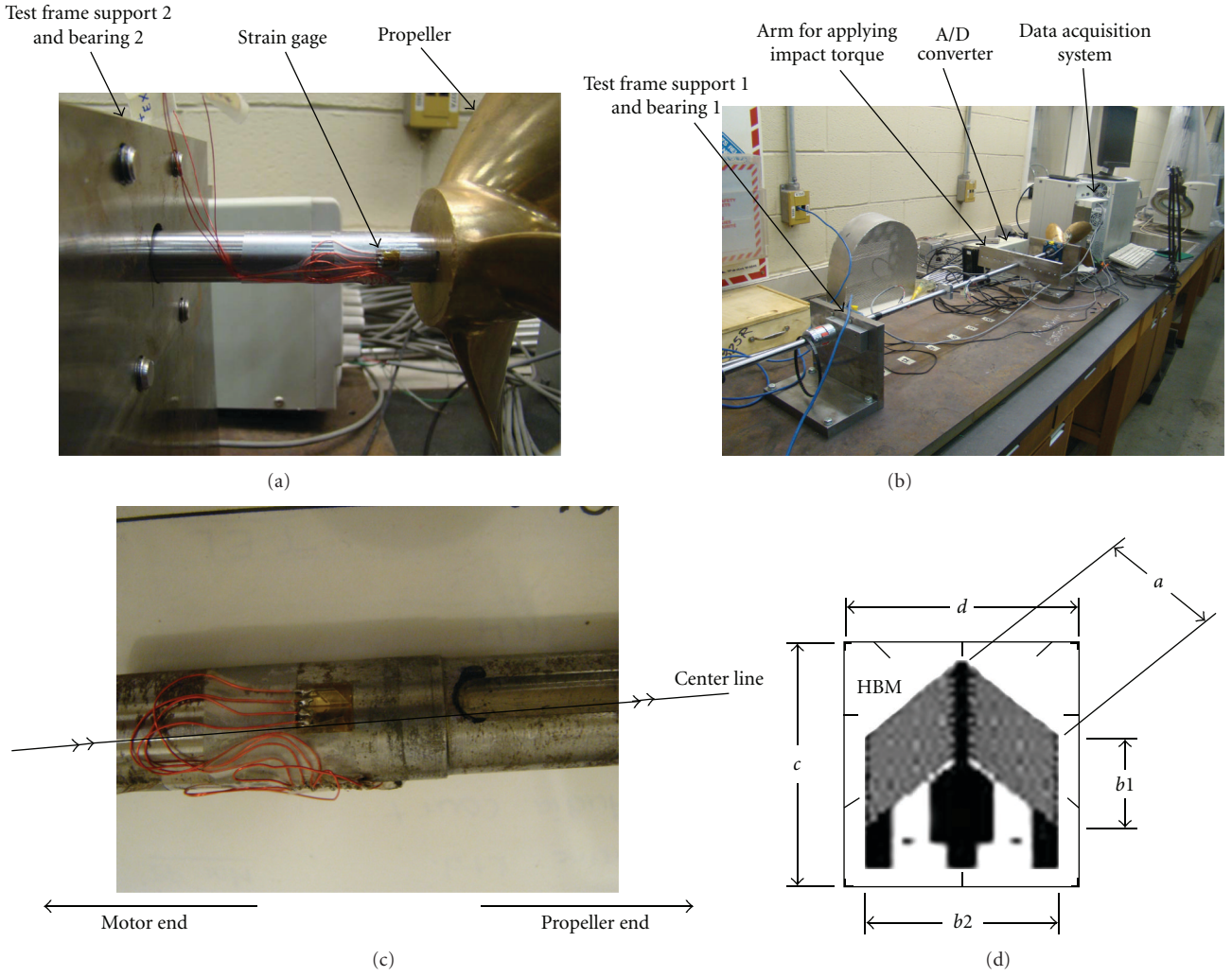

FIGURE 6: Schematic of the torsional vibration measurement instrumentation; (a) strain gage; (b) torsional load application system; (c) strain gauges used during modal tests; (d) schematic of the torsional strain gauges.

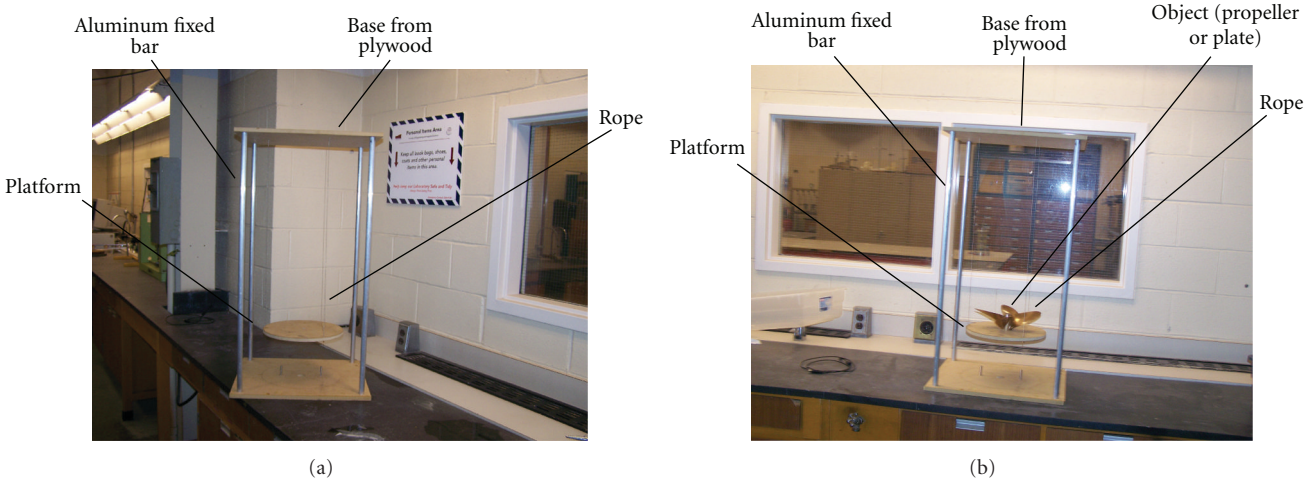

FIGURE 7: Schematic diagram of the platform suspension setup; (a) platform and (b) platform with propeller.

Table 1: Experimental and numerical values of natural frequencies for various crack depth ratios (uncorrected numerical values shown within brackets and corrected numerical results are shown with the asterisk). V: vertical and H: horizontal.

Frequency	Crack depth ratios 0.0%		10%		20%		30%	
	V	H	V	H	V	H	V	H
First	34.134 (34.338) 34.338*	43.633 (43.858) 43.858*	34.125 (34.337) 34.262*	43.515 (43.855) 43.550*	33.816 (34.337) 34.286*	43.363 (43.849) 43.046*	33.778 (34.336) 34.176*	43.343 (43.844) 42.570*
Second	76.703 (78.269) 78.269*	78.792 (80.436) 80.436*	76.657 (78.265) 77.889*	78.806 (80.425) 79.481*	76.483 (78.266) 77.953*	78.424 (80.408) 78.054*	76.195 (78.260) 76.835*	78.382 (80.392) 77.398*
Third	191.652 (190.42) 190.42*	199.499 (196.13) 196.13*	191.491 (190.42) 189.99*	199.204 (196.12) 195.04*	191.256 (190.42) 190.05*	199.069 (196.10) 193.47*	190.859 (190.41) 189.42*	199.006 (196.08) 192.17*
Fourth	367.563 (366.26) 366.26*	383.139 (382.40) 382.40*	367.282 (366.26) 365.94*	379.423 (382.39) 380.85*	365.883 (366.26) 366.03*	379.213 (382.36) 378.62*	365.752 (366.26) 365.55*	379.109 (382.33) 376.84*
Frequency	Crack depth ratios 40%		50%		60%		70%	
	V	H	V	H	V	H	V	H
First	33.556 (34.334) 33.964*	43.185 (43.841) 42.964*	33.145 (34.329) 33.563*	42.947 (43.841) 42.300*	32.774 (34.320) 32.762*	42.862 (43.841) 42.274*	31.286 (34.300) 30.964*	42.069 (43.837) 41.962*
Second	75.572 (78.248) 76.240*	78.298 (80.384) 76.412*	74.553 (78.228) 74.743*	78.214 (80.382) 76.151*	73.401 (78.186) 71.921*	77.644 (80.381) 76.059*	69.774 (78.088) 67.206*	75.896 (80.370) 75.361*
Third	190.076 (190.40) 188.34*	198.671 (196.07) 191.55*	188.763 (190.38) 186.58*	198.299 (196.07) 191.46*	187.240 (190.33) 183.81*	197.993 (196.06) 191.37*	182.790 (190.22) 179.66*	194.457 (196.05) 190.66*
Fourth	363.809 (366.25) 364.68*	378.435 (382.32) 376.03*	359.989 (366.23) 363.21*	377.565 (382.32) 375.98*	355.839 (366.19) 360.84*	376.664 (382.32) 375.92	343.971 (366.10) 357.25*	373.689 (382.30) 375.03*

to have the same moment of inertia of the shaft as that of the cracked section (to represent the longer short beam element).The results of these studies are shown later in Figure 12.

Figures 10 and 11 show the changes that occur in the experimental frequencies as the crack depth ratios change from 0 to 70% (with second-order curve fit). As observed earlier by Hamidi et al. [6], the rate of change in bending natural frequencies (shown in Figure 11) becomes noticeable when the crack depth ratio becomes greater than 20%, indicating that the rates of change in natural frequencies (with respect to crack depth ratio) seem to be a better indicator of crack presence. When the rates of frequency change (with respect to crack depth ratio) are plotted as a function of crack depth ratio it is observed that between 20% and 30% crack depth ratio, the rate of change variation is found to be 3% to 4%. Instead if frequency changes were used as the crack indicator, the changes between 20% and 30% crack depth ratio are around 0.5% to 1.0%; this is much less than that shown by the rate of change of frequency (with respect to crack depth).

These numerical results plotted in Figure 12 were correlated by comparing them with the experimental results. The first three natural frequencies were calculated for several values of the crack depth ratios [0, 0.1, 0.2, 0.3, 0.4, 0.5, 0.6, and 0.7] and for the presence of crack represented by different (twenty-nine) short shaft element lengths [0.65 (case I0), 6.65 (case I3), 12.65 (I5), 18.65 (I7), 24.65 (I9), 30.65 (I11), 36.65 (I13), 42.65 (I15), 54.65 (I19), 60.65 (I21), 66.65 (I23), 72.65 (I25), and 84.65 (case I29)] mm. Figures 12(a), 12(b), and 12(c) show the numerical and experimental results for the first, second, and third natural (nondimensional) frequencies versus crack depth ratios, respectively. Clearly, it can be seen from these figures that the first natural frequency needed a larger equivalent length shaft element to give a good agreement between numerical and experimental values. It can be seen from Figure 12(a) that the curve (given by Num. V.I_{19}) determined from numerical calculations seems to be better coincident with the curve from the experimental test results (given by experimental values). For the second and third frequencies shown in Figures 12(b) and 12(c), the curves (represented, resp., by Num. V.I_{11} and Num. V.I_9) seem to be better coincident with the curves from the experimental values (represented by Exp. values). Therefore while the first frequency needs a longer equivalent shaft element, the second and third natural frequencies need shorter equivalent shaft element lengths to give good agreement with experimental results. The above modeling of the cracked shaft (by an equivalent short shaft) gives the

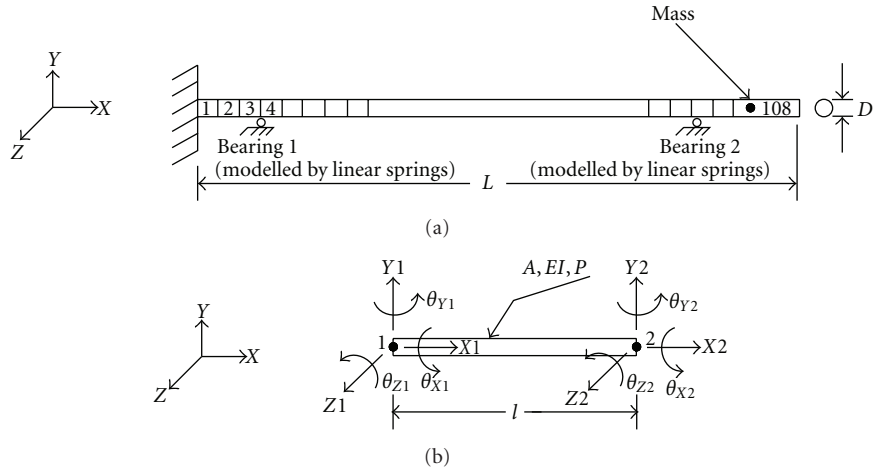

Figure 8: Schematic diagram of: (a) a shaft modeled and discretized using beam elements and (b) degrees of freedom numbering for a three-dimensional shaft element.

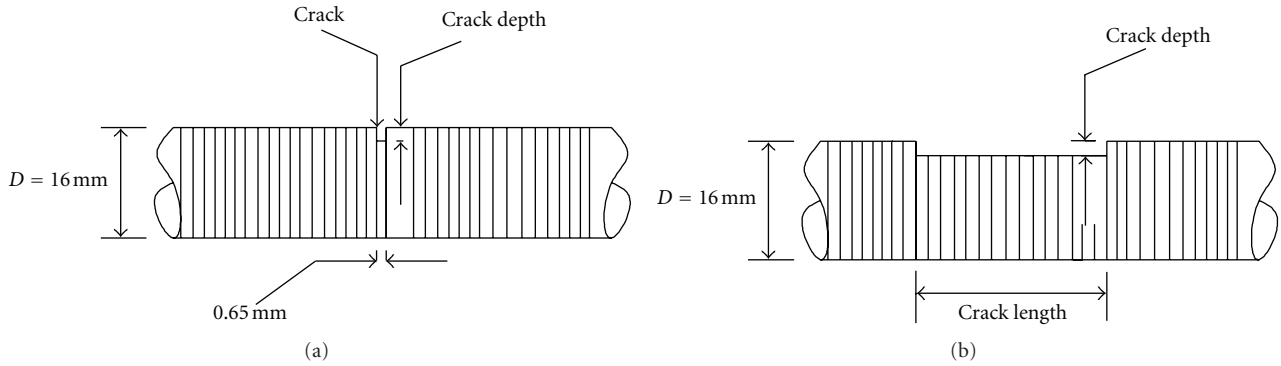

Figure 9: Schematic diagram of: (a) one element representing crack effect and (b) a wider element representing the crack effect.

best fit with the experimental results as follows: (i) for the first natural frequency, the equivalent cracked shaft length is around 54.65 mm; (ii) for the second and third natural frequencies, the values are around 30.65 and 24.65 mm.

The differences between numerical and experimental frequencies for various crack depth ratios, before and after the correction with a short shaft element for the cracked section has been made, are also given in Table 1. For the first natural frequencies the numerical values used are obtained with a short shaft element length given by Num. V.I_{19}, for the second natural frequencies the numerical values used are for those given by the short shaft element Num. V.I_{11}, and for the third natural frequencies the numerical values used are for those given by the short shaft element Num. V.I_9. It is clear from this table that the modeling of a cracked location by an equivalent short shaft element has considerably reduced the percentage differences, between the numerical and experimental values, and keeps the numerical values close to experimental values. Table 2 gives the percentage differences between the experimental and the corrected frequencies shown in Table 1. It is seen from Table 2 that the six springs' model (shown in Figure 2(b)) does not seem to be a very good model for the second vertical bending frequency, since the differences are much larger than the first and third frequencies.

Using the experimental mode shapes shown in Figures 13 to 16, the effective bending lengths (between points of contraflexures) can be taken as $((1/\sqrt{2})L_1)$ for the first mode, $((1/2)L_1)$ for the second mode, and $(L_1/(2\sqrt{2}))$ for the third mode, where L_1 is the length between the two bearing supports. Taking L_1 to be equal to 0.97 m (from Figure 1, which gives the actual span length between the two test frame supports), the effective bending lengths for the first three frequencies are obtained as 0.686 m, 0.485 m, and 0.343 m, respectively. This leads to (*effective crack length/effective bending length for the mode*) ratios of 1/12.55 for first bending mode, 1/15.83 for second bending mode, and 1/13.91 for third bending mode. Hence the value of 1/12 to 1/16 seems to give a better fit for the equivalent short length shaft ratio (= *effective crack length/effective bending length*) for the different modes. The fourth mode shape (shown in Figure 16) is not considered in the analysis owing to the following reasons. (i) The node over the bearing support seems to house shifted outside its proper location, probably due to the curve fitting procedure. (ii) Measurements are made only at fourteen locations along the length of the shaft, and this has not

Table 2: Differences between numerically and experimentally obtained frequencies, for various crack depth ratios for the equivalent shaft length modeling (values within brackets before correction).

Frequency	Crack depth ratios							
	0.0% V	10% V	20% V	30% V	40% V	50% V	60% V	70% V
First	0.59% (0.59%)	0.40% (0.62%)	1.39% (1.54%)	1.18% (1.65%)	1.22% (2.32%)	1.26% (3.57%)	0.04% (4.72%)	1.03% (8.79%)
Second	2.00% (2.00%)	1.61% (2.09%)	1.92% (2.33%)	0.84% (2.71%)	0.88% (3.42%)	0.25% (4.93%)	2.02% (6.52%)	3.68% (11.92%)
Third	0.64% (0.64%)	0.78% (0.56%)	0.63% (0.44%)	0.75% (0.24%)	0.91% (0.17%)	1.16% (0.86%)	1.83% (1.65%)	1.71% (4.06%)

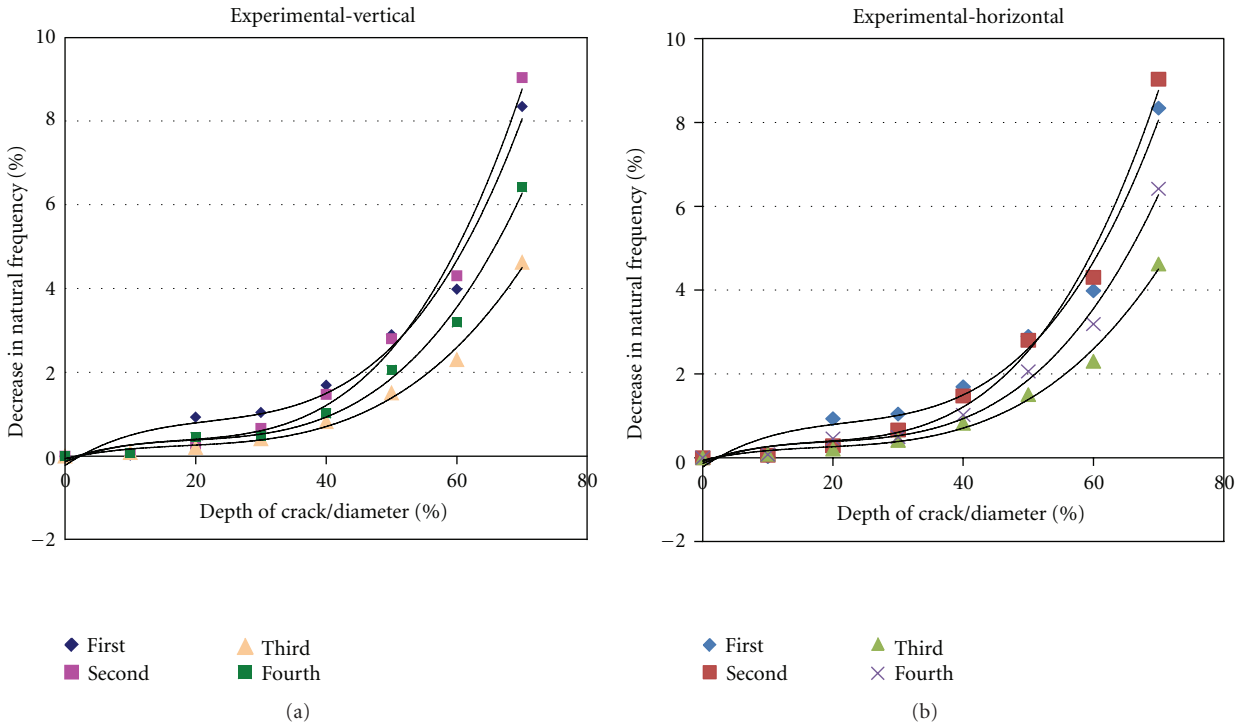

Figure 10: Depth of crack versus percent decrease in natural frequencies for experimental results: (a) vertical and (b) horizontal.

provided enough plotting points to give the proper modal shape curve. (iii) The presence of crack seems to be indicated only by the 10% curve and thereafter no appreciable change seems to occur in the plots.

The value of 1/12 to 1/16 for the equivalent short length shaft ratio can be given an alternate interpretation which will enable this ratio to be utilized in the first level crack identification scheme for shaft. When a shaft cracks, the average crack velocity in the cracked portion and the uncracked portion should be the same. Hence

$$\frac{\Delta L}{\Delta t} = \frac{L}{T_c}, \tag{8}$$

where ΔL is the effective crack length, Δt is the time taken by the considered bending wave (first record or third frequency) to cover the distance ΔL, L is the wave length of the considered wave (equal to twice the effective bending length), and T_c is the cracked frequency of the considered wave. Rearranging (7),

$$\frac{\Delta t}{T_c} = \frac{\Delta L}{L} = \frac{\Delta L}{2L_{\text{eff}}}. \tag{9}$$

Hence,

$$\frac{\Delta L}{L_{\text{eff}}} = 2\left(\frac{\Delta t}{T_c}\right). \tag{10}$$

According to Rao [20] in a time-domain numerical integration procedure using finite-difference schemes, the solution becomes unconditionally stable and reasonably accurate when the $\Delta t/T_{\text{uc}}$ ratio is smaller than 1/20 to 1/40. From Table 1, it can be seen that when crack depth ratio is around 40%, the T_{uc}/T_c is approximately 1.02 for the first mode and 1.01 for the second and third modes. Hence $\Delta t/T_{\text{uc}}$ ratio can

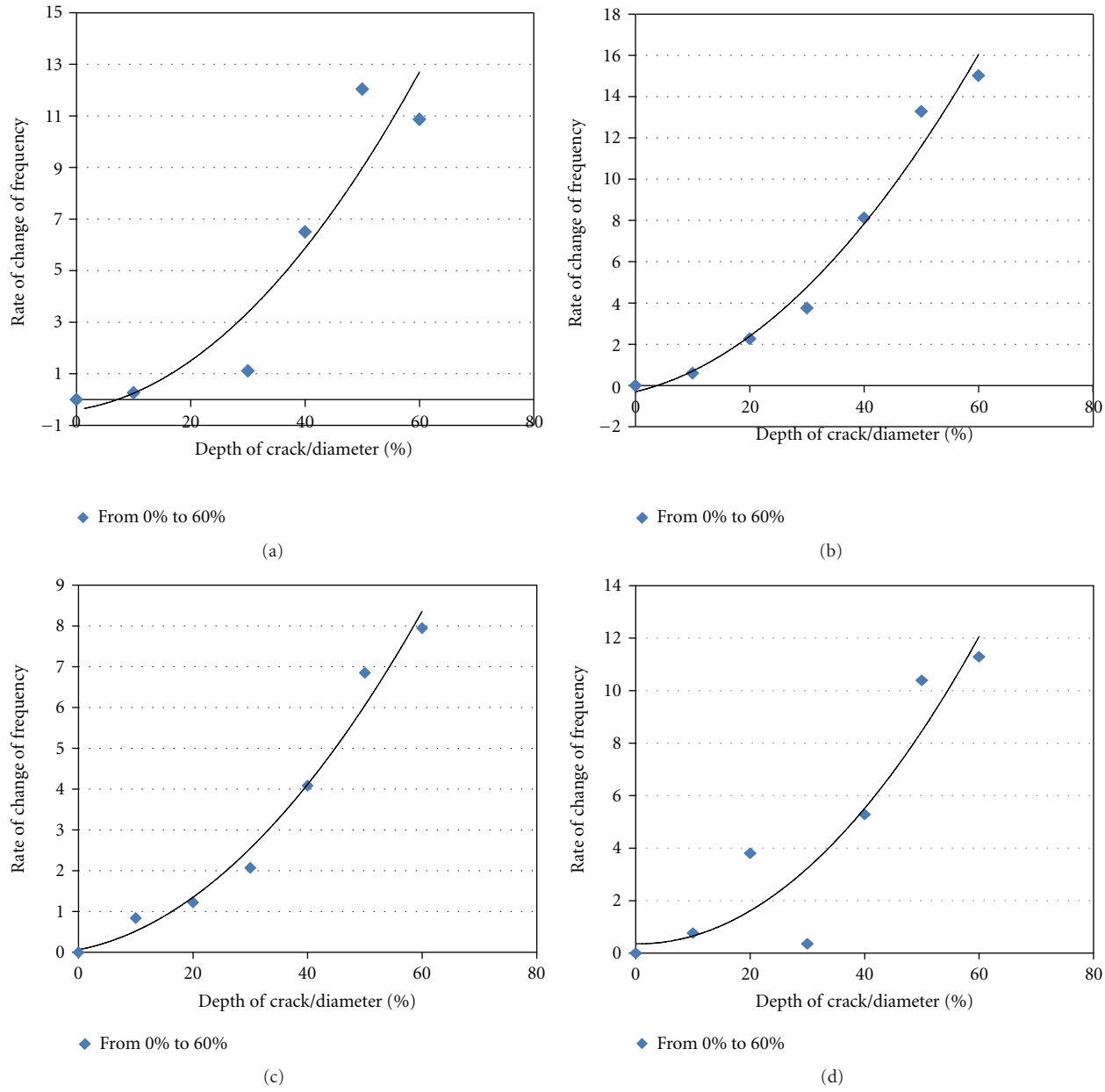

Figure 11: Rate of change of frequency (with respect to crack depth ratio) versus crack depth ratio of the first four frequencies: (a) mode one; (b) mode two; and (c) mode three.

be expected to be smaller than 1/19.6 to 1/38.4. Hence (10) can be expressed as

$$\frac{1}{9.8} < \frac{\Delta L}{L_{\text{eff}}} < \frac{1}{19.2}, \tag{11}$$

which is approximately the ratio obtained from the experimental values. Consequently a finite element analysis could be carried out with the ratio of (effective crack length/effective bending length) of (1/12.0) to (1/16) and the cracked frequency of rotating shafts be obtained for a crack depth ratio 40%. When the measured frequency of the rotating shaft reduces below this value for the first three modes, then one can be invariably sure to say that there is a crack or damage in the rotating shaft and carry out a detailed inspection on the rotating shaft to locate the crack.

Figures 13 to 16 give the experimental data plots given by LMS Test Laboratory software, showing the experimental mode shapes for the various crack depth ratios (0.0 to 0.7), for the first four frequencies (plotted as a function of modal amplitudes versus accelerometer location). Since only vertical frequencies are of concern, we consider only Figures 13(a), 14(a), and 15(a). It is seen from these three figures that the identifier of the mode shape change due to crack is shown better by the third mode shape than the other two mode shapes; hence the crack presence can be best detected by monitoring the third vertical bending mode of the rotor

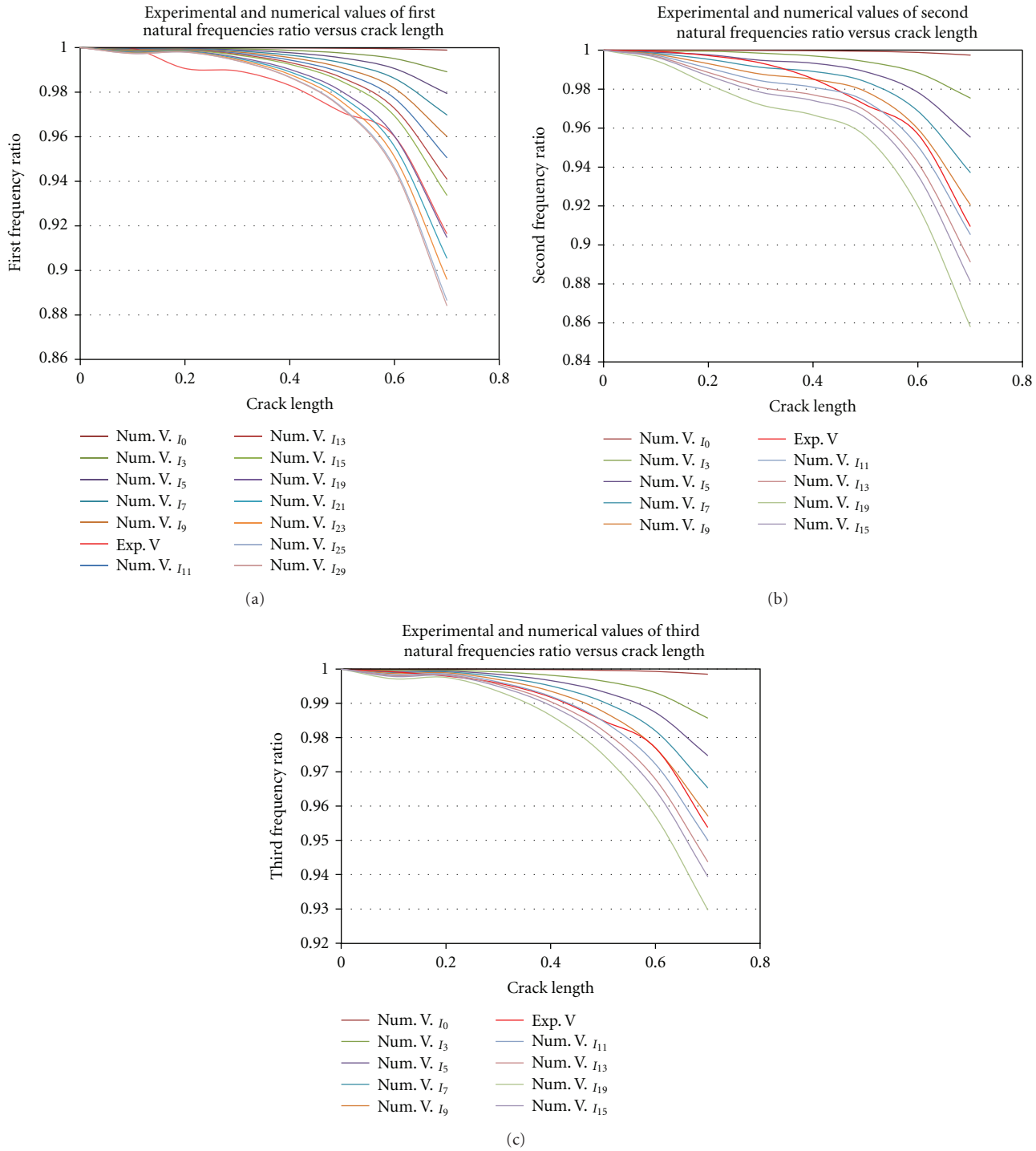

FIGURE 12: Experimental and numerical values of nondimensionalized vertical natural frequencies versus crack depth ratios; (a) first natural frequency; (b) second natural frequency; and (c) third natural frequency.

shaft. It should also be noticed that the changes in mode shapes shown in Figure 15(a) (for the third mode) are higher than the frequency changes shown in Figure 12. This can be appreciated if it can be noticed that this case (third mode) is similar to the case of a fixed-simply supported case (or a cantilever case), where the crack occurs around the fixed edge (bearing 2).

Figure 17(a) shows the plot of the depth of crack and percent change (decrease) in torsional natural frequencies for experimental measurements. Figure 17(a) shows that the changes in the first torsional frequency give a much better indication of the crack presence even during the starting of the crack. This is better shown through Figure 17(b) which plots the rate of change of torsional frequency (with respect

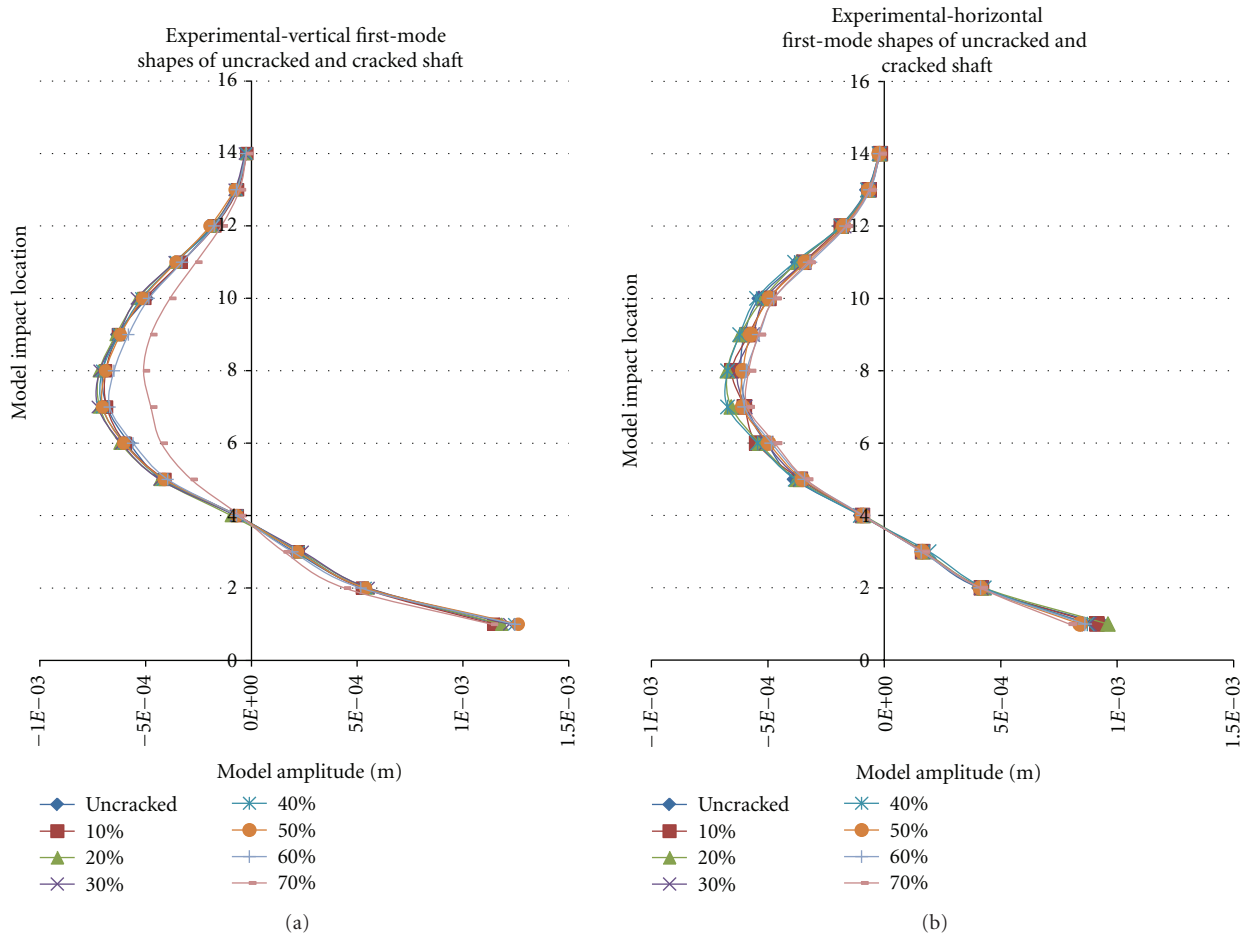

Figure 13: First-mode shapes of uncracked and cracked shaft from experimental work: (a) vertical and (b) horizontal.

Table 3: Theoretical and experimental values of mass moment of inertia and torsional natural frequencies.

Mass moment of inertia for platform, kg·m^2		Mass moment of inertia for platform with propeller, kg·m^2	Mass moment of inertia for propeller, kg·m^2	Total mass moment of inertia (propeller + plate* + shaft**), kg·m^2	Torsional natural frequency for uncracked shaft w_n, Hz	
Theoretical	Experimental	Experimental	Experimental	Theoretical and experimental	Theoretical	Experimental
(a)	(b)	(c)	(d) = (c) − (b)			
7.746×10^{-3}	7.571×10^{-3}	1.163×10^{-2}	4.057×10^{-3}	5.639×10^{-3}	43.04	43.72

* $J_{plate} = 1.5232 \times 10^{-3}$ kg·m^2 (by experimental measurements); ** $J_{shaft} = 1.5232 \times 10^{-3}$ kg·m^2 (by theory).

to crack depth ratio) versus the crack depth ratio. It is seen that the rate of change in the first torsional frequency (with respect to crack depth ratio) versus crack depth ratio is much higher (at a crack depth ratio of 10%, the rate of change of frequency with respect to crack depth ratio is nearly 10.0%) whereas the rate of change of bending frequencies during the earlier stage of crack initiation and growth is much less (at a crack depth ratio of 10%, the rate of change of frequency with respect to crack depth ratio is only 1.0%); refer to Figures 12 and 17(b). This could be easily understood since the influence of cracking on torsional inertia (due to its larger influence along the skin surface of the cylindrical shaft than its depth) will be much higher than the bending inertia and the consequent changes in the rate of frequency change. Hence the rate of change of torsional frequency could very well be used as a very good indicator of the presence of any small crack.

Considering Table 3 and value of torsional natural frequency of experimental measurements for uncracked shaft, it can be seen that the error between analytical and experimental values is less than 1.57%, indicating that the experimental measurements seem to have been done very carefully.

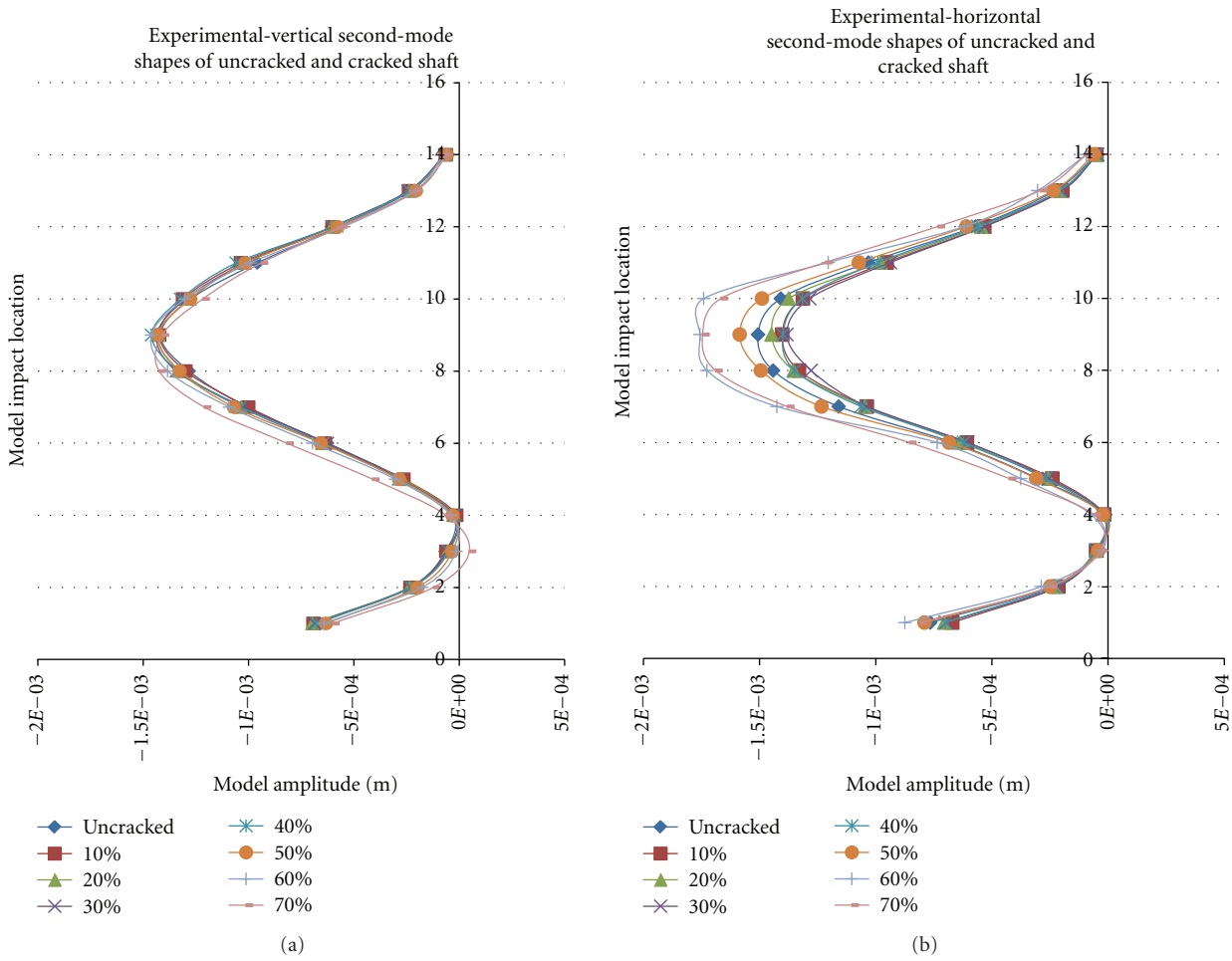

Figure 14: Second-mode shapes of uncracked and cracked shaft from experimental work: (a) vertical and (b) horizontal.

6. Conclusions

From the above experimental and numerical studies, the following contributions from this study can be presented.

(1) In this paper, five spring models were developed to represent the ball-bearing support effect, namely, six, eight, and twelve springs. It is seen that bearings with six springs, shown in Figure 2(a), give the best agreement between experimental and numerical results. This is due to the fact that that this model closely represents the elasticity effects that exist between the two tight screws that connect the inner bearing to the cylindrical shaft and elasticity of the support provided by the two frame supports 1 and 2.

(2) The values of the experimental natural frequencies for vertical and horizontal transverse vibrations were not the same for all the different pair of (vertical and horizontal) modes; consequently the difference in modeling the two orthogonal bearing support contacts by linear springs becomes very important so as to make the numerical values closer to the measured experimental values; this has to be done very carefully.

(3) From the modeling of a crack, in a cracked shaft, by an equivalent short beam, the best fit for the length of a shaft element for first natural frequency is about 54.65 mm while the best fit for second and third natural frequencies is between 30.65 mm and 24.65 mm, respectively. This gives an approximate ratio (= *effective crack length/effective bending length for the mode*) of 1/12 to 1/16 for different modes. This also seems to be corroborated by the digitized time interval requirements for accuracy in finite-difference-related numerical integration. The above relationship could be used as a first-level inspection scheme for determining the presence of cracking in a rotating shaft.

(4) The third-mode shape could be used as a good indicator of the presence of a crack in the shaft. This gives a much higher variation in mode shapes than the changes in frequencies that occur due to the presence of the crack.

(5) Vibration analysis for experimental results was successful in detecting the presence of a crack. These results show that it is possible to detect a crack, around the crack depth ratio of 20%, when the rates of

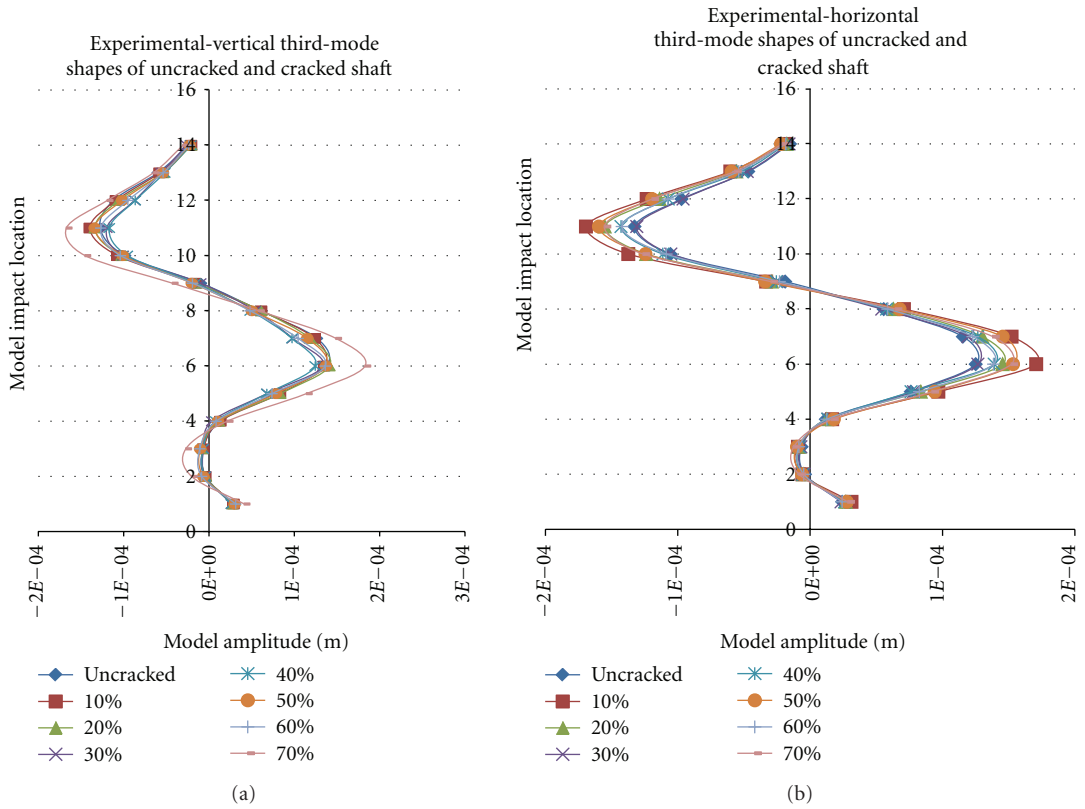

Figure 15: Third-mode shapes of uncracked and cracked shaft from experimental work: (a) vertical and (b) horizontal.

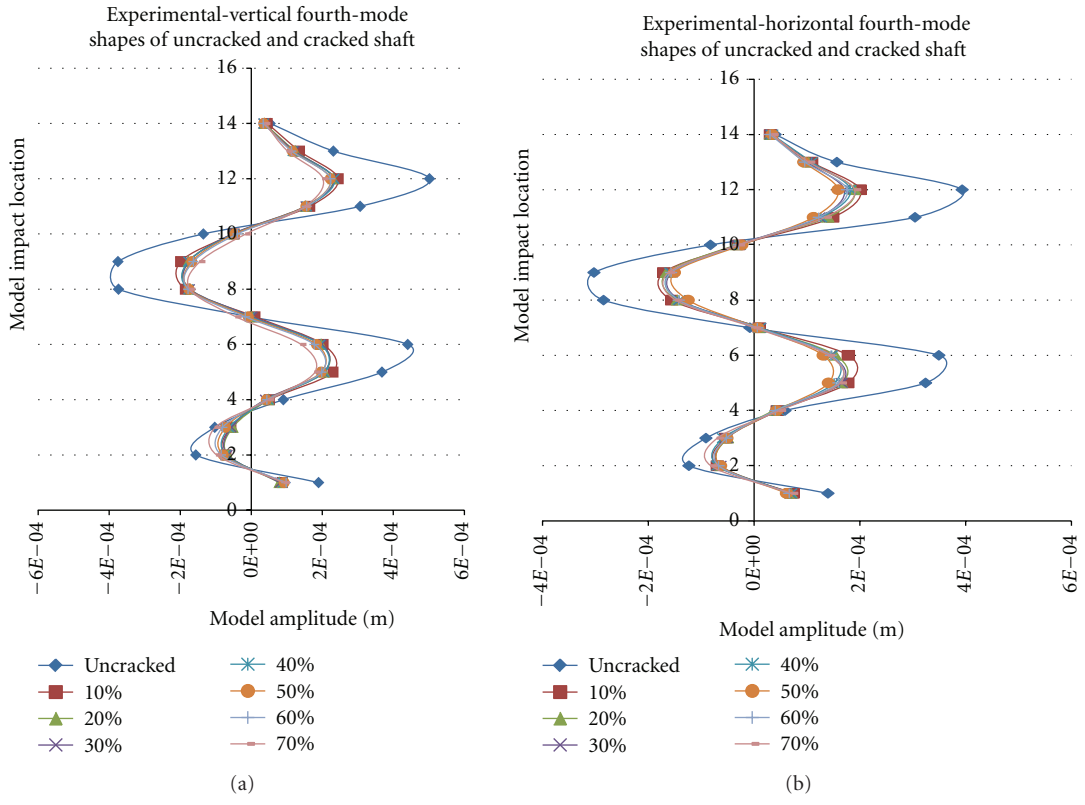

Figure 16: Fourth-mode shapes of uncracked and cracked shaft from experimental work: (a) vertical and (b) horizontal.

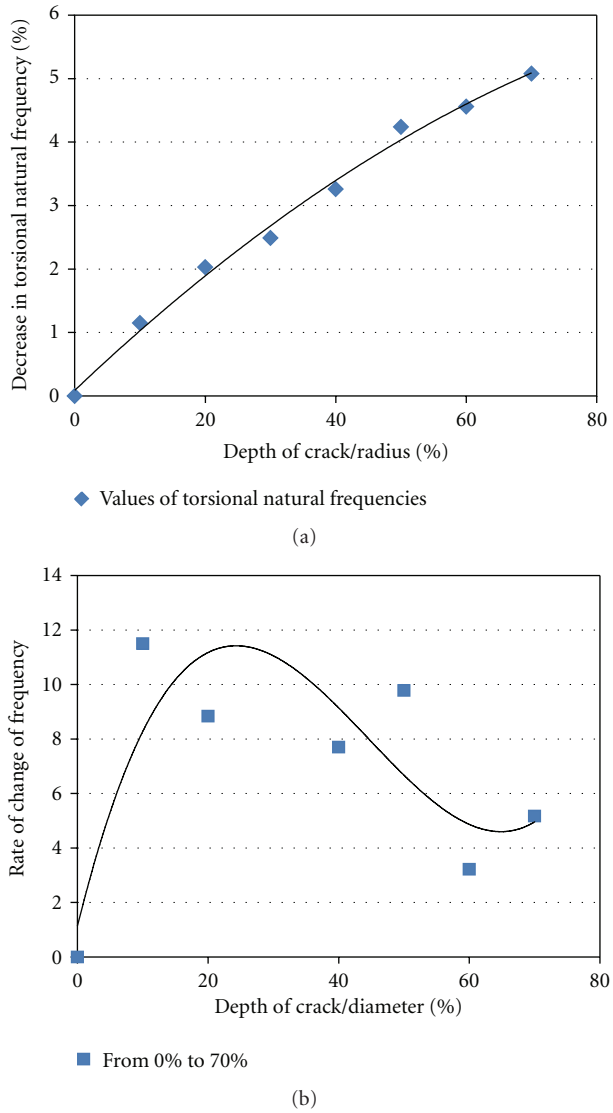

FIGURE 17: (a) Depth of crack and percent decrease in torsional natural frequencies for experimental results and (b) rate of change of frequency (with respect to crack depth ratio) versus crack depth ratio.

frequency change (as a function of crack depth ratio) are plotted as a function of crack depth ratio (between 20% and 30% crack depth ratios, the rate of change variation is found to be 3% to 4%). Instead if frequency changes were used as the crack indicator, then the changes are much smaller (between 20% and 30% crack depth ratios, the change in frequency ratio is around 0.5% to 1.0%) than that shown by the rate of change of frequency (with respect to crack depth).

(6) Monitoring the first torsional frequency [with regards to its rate of change (with respect to crack depth ratio)] gives a much better indication of the crack presence (at a 10% crack depth ratio, the rate of change of frequency is around 10%) than the monitoring of bending frequencies for its rate of change with respect to crack depth ratio (at a 10% crack depth ratio, the rate of change of frequency is around 1%).

Acknowledgment

The authors would like to express their sincere gratitude to the staff of the Structural Lab of the Faculty of Engineering and Applied Science at the Memorial University.

References

[1] J. Wauer, "On the dynamics of cracked rotors: a literaturesurvey," *Applied Mechanics Reviews*, vol. 43, no. 1, pp. 13–17, 1990.

[2] A. D. Dimarogonas, "Vibration of cracked structures: a state of the art review," *Engineering Fracture Mechanics*, vol. 55, no. 5, pp. 831–857, 1996.

[3] G. Sabnavis, R. G. Kirk, M. Kasarda, and D. Quinn, "Cracked shaft detection and diagnostics: a literature review," *The Shock and Vibration Digest*, vol. 36, no. 4, pp. 287–296, 2004.

[4] R. Q. Munoz, J. A. S. Ramirez, and J. S. Kubiak, "Rotor modal analysis for a rotor crack detection," in *Proceedings of the 15th International Modal Analysis Conference (IMAC' 97)*, vol. 1, pp. 877–879, February 1997.

[5] G. D. Gounaris and C. A. Papadopoulos, "Crack identification in rotating shafts by coupled response measurements," *Engineering Fracture Mechanics*, vol. 69, no. 3, pp. 339–352, 2002.

[6] L. Hamidi, J. Piaud, and M. Massoud, "A study of crack influence on the modal characteristics of rotors," in *Proceedings of the International Conference on Vibrations in Rotating Machinery*, pp. 283–288, Bath, UK, 1992, No. C432/066.

[7] T. C. Tsai and Y. Z. Wang, "Vibration analysis and diagnosis of a cracked shaft," *Journal of Sound and Vibration*, vol. 192, no. 3, pp. 607–620, 1996.

[8] A. Zakhezin and T. Malysheva, "Modal analysis rotor system for diagnostic of the fatigue crack," in *Proceedings of the Condition Monitoring Conference*, St. Catherine's College, Oxford, UK, 2001.

[9] S. A. Adewusi and B. O. Al-Bedoor, "Detection of propagating cracks in rotors using neural networks," in *Proceedings of the American Society of Mechanical Engineers, Pressure Vessels and piping Division Conference*, vol. 447, pp. 71–78, Vancouver, Canada, August 2002.

[10] S. Prabhakar, A. S. Sekhar, and A. R. Mohanty, "Detection and monitoring of cracks using mechanical impedance of rotor-bearing system," *Journal of the Acoustical Society of America*, vol. 110, no. 5, pp. 2351–2359, 2001.

[11] P. Pennacchi and A. Vania, "Diagnostics of a crack in a load coupling of a gas turbine using the machine model and the analysis of the shaft vibrations," *Mechanical Systems and Signal Processing*, vol. 22, no. 5, pp. 1157–1178, 2008.

[12] L. S. Dorfman and M. Trubelja, "Torsional monitoring of turbine-generators for incipient failure detection," in *Proceedings of the 6th EPRI Steam Turbine/Generator Workshop*, pp. 1–6, St. Louis, Mo, USA, August 1999.

[13] S. H. Cho, S. W. Han, C. I. Park, and Y. Y. Kim, "Noncontact torsional wave transduction in a rotating shaft using oblique magnetostrictive strips," *Journal of Applied Physics*, vol. 100, no. 10, pp. 104903–104906, 2006.

[14] H. J. Petroski, "Simple static and dynamic models for the cracked elastic beams," *International Journal of Fracture*, vol. 17, no. 4, pp. R71–R76, 1981.

[15] A. Rytter, *Vibrational based inspection of civil engineering structures*, Ph.D. thesis, Department of Building Technology and Structural Engineering, University of Aalborg, Aalborg, Denmark, 1993.

[16] "McMaster-Carr (Princeton, New Jersey, USA) supplies products (including bearings) used to maintain manufacturing plants and large commercial facilities worldwide," http://www.mcmaster.com/.

[17] ANSYS 13, *Section 3.12.7 on Limitations of Lumped Matrix Formulation with Beam, Pipe, or Shell Elements*, SAS IP, Cheyenne, Wyo, USA, 13th edition, 2010.

[18] Laboratory Handout, *Determination of Moment of Inertia*, Department of Mechanical Engineering, Dalhousie University, Halifax, NS, Canada, 2007.

[19] X. Yang, *Vibration based crack analysis and detection in beam using energy method*, Ph.D. thesis, Faculty of Engineering, Memorial University, St. John's, NL, Canada, 2001.

[20] S. Rao, *Mechanical Vibrations*, Addison Wesley, New York, NY, USA, 1995.